# The Australian Air Quality Forecasting System. Part I: Project Description and Early Outcomes

M. E. COPE,*,+ G. D. HESS,# S. LEE,* K. TORY,# M. AZZI,+ J. CARRAS,+ W. LILLEY,+ P. C. MANINS,* P. NELSON,** L. NG,& K. PURI,* N. WONG,& S. WALSH,& AND M. YOUNG@

*CSIRO Atmospheric Research, Aspendale, Victoria, Australia
+CSIRO Energy Technology, Newcastle, New South Wales, Australia
#Bureau of Meteorology Research Centre, Melbourne, Victoria, Australia
@Department of Environment and Conservation (NSW), Lidcombe, New South Wales, Australia
&Environment Protection Agency of Victoria, Melbourne, Victoria, Australia
**Graduate School of the Environment, Macquarie University, North Ryde, New South Wales, Australia

(Manuscript received 28 November 2002, in final form 29 July 2003)

ABSTRACT

The Australian Air Quality Forecasting System (AAQFS) is the culmination of a 3-yr project to develop a numerical primitive equation system for generating high-resolution (1–5 km) short-term (24–36 h) forecasts for the Australian coastal cities of Melbourne and Sydney. Forecasts are generated 2 times per day for a range of primary and secondary air pollutants, including ozone, nitrogen dioxide, carbon monoxide, sulfur dioxide, and particles that are less than 10 $\mu$m in diameter (PM10). A preliminary assessment of system performance has been undertaken using forecasts generated over a 3-month demonstration period. For the priority pollutant ozone it was found that AAQFS achieved a coefficient of determination of 0.65 and 0.57 for forecasts of peak daily 1-h concentration in Melbourne and Sydney, respectively. The probability of detection and false-alarm rate were 0.71 and 0.55, respectively, for a 60-ppb forecast threshold in Melbourne. A similar level of skill was achieved for Sydney. System performance is also promising for the primary gaseous pollutants. Further development is required before the system can be used to forecast PM10 confidently, with a systematic overprediction of 24-h PM10 concentration occurring during the winter months.

## 1. Introduction

Over the past decade results from a number of epidemiological studies into health effects and air pollution have suggested associations between daily mortality/morbidity rates and ambient air pollution levels. For example, a study recently conducted in Melbourne, Australia, found links between ozone, nitrogen dioxide, carbon monoxide, and fine particles concentrations and increases in daily mortality (EPA Victoria 2000). The strongest associations were observed for ozone and nitrogen dioxide. In the case of ozone, a 1-ppb increase in the 4-h ozone concentration was associated with a 0.27% increase in all-age respiratory mortality for that day.

A two-pronged approach has been adopted by environmental authorities to mitigate the health impacts of air pollution.

1) Long-term strategic policies to curtail sources of air pollution are developed and implemented.
2) Authorities are increasingly looking to improve their capacity to forecast pollution events with a view to issuing warnings to the population. This may be coupled with education programs to encourage behaviors to curtail the emissions of air pollutants on these days.

In this paper, the discussion is related to the second response and considers the development and application of a state-of-the-art numerical air pollution forecasting system for short-term forecasting in the local and regional airsheds surrounding the coastal cities of Melbourne and Sydney in Australia (Fig. 1). Known as the Australian Air Quality Forecasting System (AAQFS), the system is the outcome of a 3-yr project sponsored by Environment Australia. The project spans organizational boundaries, involving the close cooperation and commitment of resources from four separate government organizations.

AAQFS is a numerical air quality forecasting system (NAQFS). As such, forecasts for primary and secondary pollutants are generated through numerical solution of the governing equations for mass, momentum, and energy of the atmosphere [numerical weather prediction (NWP)], and through solution of equations describing

*Corresponding author address:* M. E. Cope, CSIRO Atmospheric Research, PMB 1, Aspendale VIC 3195, Australia.
E-mail: martin.cope@csiro.au

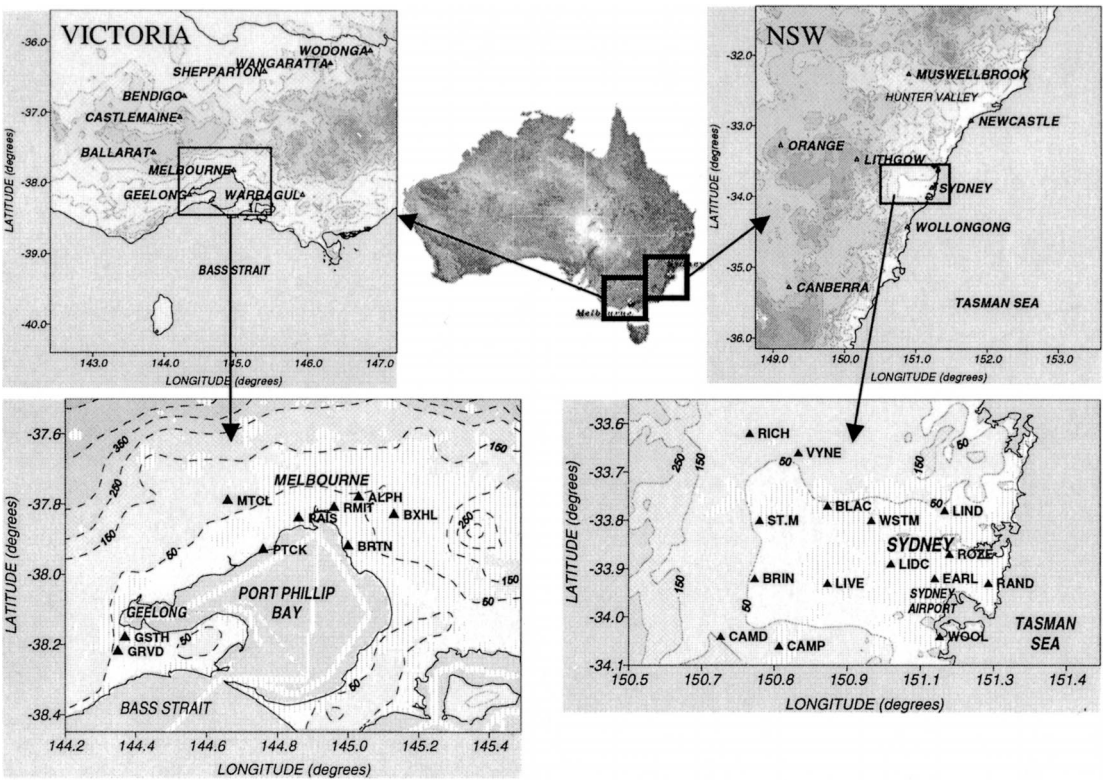


FIG. 1. Location of AAQFS CTM domains. The regional grids of (top left) Victoria and (top right) NSW have a horizontal spacing of 0.05° (approximately 5 km), and the nested urban grids of (bottom left) Port Phillip and (bottom right) Sydney basin have a horizontal spacing of 0.01° (approximately 1 km). All grid plots show contours of topographic relief (100-m intervals). In addition, the urban grids show the distribution of commercial and domestic sources. Also shown on the urban grids are the locations of air quality monitoring stations. Port Phillip: Alphington (ALPH), Brighton (BRTN), Box Hill (BXHL), Mount Cottrell (MTCL), Paisley (PAIS), Point Cook (PTCK), Geelong South (GSTH), and Grovedale (GRVD); Sydney basin: Camden (CAMD), Campbelltown (CAMP), Bringelly (BRIN), Liverpool (LIVE), Lidcombe (LIDC), Earlwood (EARL), Randwick (RAND), Woolooware (WOOL), St. Mary's (ST.M), Rozelle (ROZE), Blacktown (BLAC), Westmead (WSTM), Lindfield (LIND), Vineyard (VYNE), and Richmond (RICH).

the transport and physiochemical transformation of gaseous and particle pollutants [chemical transport modeling (CTM)]. The use of an NAQFS for high-resolution multispecies forecasting is a recent trend, made practical by the increasing availability of affordable high-performance computing platforms. Early examples of operational NAQFS are provided by Ohara et al. (1998), who reported on urban-scale forecasts of photochemical smog in the Chiba prefecture in Tokyo, Japan; Rufeger et al. (1997) and Walter (1997), who undertook traffic and air pollution forecasts (2-km grid) in Berlin, Germany; McHenry et al. (2000) who have been generating photochemical smog forecasts for the eastern half of the United States (15-km grid); Brandt et al. (2001), who forecast air quality down to street canyon level in Denmark; and Draxler (2000), who compared the performance of regression, box, and three-dimensional transport models for ozone forecasts in Houston, Texas.

The NAQFS can be contrasted with alternative systems, such as those based on statistical regression, that use predictants, such as the current air quality, and forecasts of mean sea level pressure, ventilation, and temperature. This category of forecasting system has now been in use for decades and has often attained a high degree of refinement. For example, a semiautomated expert system for forecasting summer photochemical smog events and winter visibility events has operated in Melbourne since the early 1980s (Morgan 1986) and continues to be evaluated and improved (Dewundege 2001). Given the widespread use of statistical/objective forecasting schemes, one of the challenges of NAQFS development is to demonstrate that the additional cost of operating a computationally intensive numerical system is outweighed by the usefulness of the delivered forecast products.

The principal goals of the AAQFS project are as follows. 1) Twice-daily, 24–36-h air quality forecasts [to be delivered to the Environment Protection Authorities (EPA) by 0900 and 1500 local time], at an inner resolution sufficient to provide suburban-scale spatial discrimination [$O$(1 km)], are generated. 2) Forecasts for a range of pollutants are generated, including ozone ($O_3$), nitrogen dioxide ($NO_2$), particles [particles that are less than 10 $\mu$m in diameter (PM10), particles that

are less than 2.5 $\mu$m in diameter (PM2.5), and visibility], carbon monoxide (CO), sulfur dioxide ($SO_2$), and ubiquitous air toxics, such as benzene and 1,3-butadiene. The health impacts associated with air toxic compounds appear to be related to long-term (lifetime) exposure, and so the model forecasts for these parameters are archived for future studies. 3) For educational purposes, the facility is provided to generate a ''green'' emissions forecast in which, for example, motor vehicle emissions are reduced by 25% following a (hypothetical) concerted public move to alternative forms of transport in response to current or forecast deleterious air quality. 4) The system is demonstrated during the Sydney 2000 Olympics and the following summer and winter.

AAQFS has been in development since 1997, following a demonstration of feasibility in Perth, western Australia (Cope and Hess 1998). A pilot system commenced operation in Sydney, New South Wales (NSW), in 1998, using operational meteorological forecasts generated by the Australian Bureau of Meteorology (BoM), simplified inventories (diurnal cycle but without weekly/seasonal/meteorological dependencies), and a modified version of the Carnegie Mellon–California Institute of Technology photochemical airshed model (Harley et al. 1993). The pilot system provided experience in the practicalities of daily operational forecasting and indicated the potential of the numerical modeling approach (Hess et al. 2000).

A demonstration system was implemented in August 2000, in time for the Sydney 2000 Olympics. The demonstration system differed from the pilot system in that it used contemporary emission inventories with full meteorological–weekday/weekend/seasonal dependencies, a custom-built chemical transport model, key modifications to BoM's operational meteorological forecasting system, and upgrades to the data visualization and validation systems.

The demonstration system is introduced in this paper. A description of the system design is provided in the next section. This is followed in section 3 by the presentation of results for a 3-month period. This period has proved sufficient to demonstrate the promise of the NAQFS approach and also to highlight areas in which further development work has to be undertaken. The latter is discussed in section 4. Two detailed case studies demonstrating performance (with emphasis on the veracity of the meteorological predictions) are presented in companion papers (Hess et al. 2004; Tory et al. 2004).

## 2. System design

A schematic diagram of AAQFS is given in Fig. 2. The nexus of AAQFS is an operational numerical weather prediction system, which provides 36-h meteorological forecasts. BoM's Limited Area Prediction System (LAPS; Puri et al. 1998) comprises the NWP for AAQFS. The LAPS suite generates forecasts on several nested domains, starting at 0.375° resolution for broadscale guidance (which is nested in the BoM global model), with finer features generated by a continentwide version operating at a resolution of 0.125°. The air quality applications operate within two very finescale versions of LAPS with a horizontal grid spacing of 0.05° (approximately 5 km). These are run twice daily (commencing at 1200 and 0000 UTC) and generate 36-h forecasts for two domains—one approximately covering the state of Victoria and the other a significant proportion of NSW.

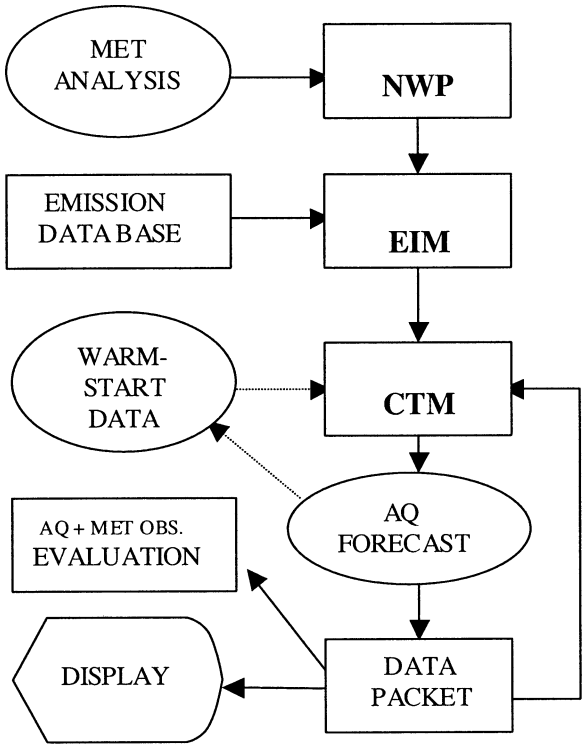


FIG. 2. Schematic of AAQFS layout showing the relationship between model components and databases.

The Emissions Inventory Module (EIM; Ng et al. 2000) was developed by EPA Victoria, with assistance from the Department of Environment and Conservation (NSW) (hereinafter DEC). The EIM provides emissions forecasts for a range of air pollutants including CO, $NO_x$, PM10, $SO_2$, volatile organic compounds (VOC), ammonia, benzene, 1,3-butadiene, and formaldehyde. Particles are speciated into discrete compounds and size fractions, and VOC are speciated into individual Carbon Bond IV (CB-IV; Gery et al. 1989) species. The emissions model consists of seven submodels: point source, area source, motor vehicle, biogenics, prescribed burning and wildfires, sea salt aerosol, and windblown dust. The emissions forecast is coupled to the NWP forecast through the use of day-specific variations in source groups subject to meteorological influences. Meteorological dependency is divided into two groups—(i) weak dependency, in which emissions are calculated as a function of basinwide and/or daily average temperatures or temperature gradients, and (ii) strong dependency, in

which emissions are calculated as a function of near-surface hourly gridpoint meteorological conditions. For example, emissions from domestic wood combustion are a source group with weak meteorological dependency. Basinwide emissions are adjusted linearly according to the predicted daily average temperature using an algorithm developed by Ng and Minchin (2000). Emission groups categorized as having strong meteorological dependency are calculated online in the CTM (Fig. 2). These groups are biogenic [with emission rates for eucalypts and grasses taken from a study by Nelson et al. (2001)], sea salt (Monahan et al. 1986), and windblown dust (Lu and Shao 2001). Emissions of particles, $NO_x$, and VOC from wildfires and prescribed burns are estimated using an algorithm adapted from Ferguson et al. (1998). Plume rise from point-source and wildfire emissions is also calculated in situ. Note that the windblown dust and the wildfire/prescribed burns algorithms were not operational during the study period presented in this paper.

The CTM comprises a multiscale Eulerian regional–urban photochemical model, with simple extensions to treat the transport and deposition of size-lumped particle species. The governing equation for the CTM is the semiempirical advection–diffusion equation for reactive species, written in scaled form (Toon et al. 1988). A spherical coordinate system is used in the horizontal direction, and a scaled pressure coordinate system is used in the vertical direction, thus matching the coordinate systems used in LAPS.

Two photochemical mechanisms are available for use in the CTM: Generic Reaction Set (GRS; Azzi et al. 1992) and CB-IV (Gery et al. 1989), the latter incorporating modifications recommended by Adelman (1999). The results presented in this paper are for the GRS mechanism, a highly condensed and simplified equation set (seven species and seven reactions) that, for a prescribed parameter space, can be tuned to generate results comparable to more comprehensive mechanisms (Venkatram et al. 1994).

The particle scheme is currently limited to parameterizing the processes of emission, transport, and deposition of primary anthropogenic and natural particle sources. A simple sectional-based (eight bins) emission–transport–deposition system is used for modeling the particle species.

The design of the CTM is predicated on the fact that photochemical smog (with ozone as the air quality indicator) is the most critical air pollutant group for Melbourne and Sydney. A secondary priority is to forecast events of high particle loading. In either city, the worst episodes of particle pollution generally result from large primary particle sources—domestic wood combustion and motor vehicles under conditions of low ventilation in the winter, and smoke from wildfires and controlled burns or windblown dust in the summer (Manins et al. 2002). A tertiary priority is to forecast other (generally less critical) urban pollutants, such as CO and $SO_2$, and to accumulate a longitudinal database of forecast fields for the air toxic pollutants.

The CTM has been designed to run with multiple online one-way nesting for an arbitrary number of grid nests. The grid configurations for the Victorian and NSW CTM domains are shown in Fig. 1. Regional grids ($98 \times 98$ north–south and east–west) with a grid spacing of $0.05^\circ$ ($\approx$5 km) extend over large proportions of the states of Victoria and NSW. Nested within these regional grids are urban grids (Port Phillip, $130 \times 96$; Sydney basin, $98 \times 56$) with a spacing of $0.01^\circ$ ($\approx$1 km). The CTM domains are configured with 17 nonuniform levels in the vertical direction, extending to $\approx$4 km, with the lowest level centered on 10 m. The $0.05^\circ$ LAPS meteorological fields are linearly interpolated to the $0.01^\circ$ CTM urban domains. While having a $0.05^\circ$ grid for the meteorological calculations and a $0.01^\circ$ grid for the urban chemical calculations is not optimal, experience has shown that this procedure improves the forecasts by allowing better resolution of the emissions. We note that because the interpolated winds are constrained to be mass consistent, the errors incurred because of grid inconsistency should be minimal. However, our plans are to improve the resolution of the meteorological fields to $0.01^\circ$, when the operational nonhydrostatic meteorological model becomes available.

In Australia, the large urban centers are isolated and long-range transport of pollutants is not as significant as it is in other more densely populated parts of the world. As a consequence, it is possible to specify a set of generic, clean background trace species concentrations for the 5-km grid boundaries. In any event, the external boundaries are sufficently far from the inner domain as to have minimal (if not zero) effect on the development of peak concentrations within the urban plume in the inner domain.

From Fig. 2 it can be seen that the demonstration system is configured in an offline mode relative to the NWP, with no feedback between the CTM and NWP calculations. Note, however, the presence of an optional feedback loop to the CTM. The following two modes of CTM initialization are available in the demonstration system: ''cold start,'' in which the pollutant fields are initialized using a generic set of continental and oceanic concentration profiles; or ''warm start,'' in which the pollutant concentration fields of the previous forecast are used to initialize a downstream air quality forecast. Our experience and the experience of others (e.g., McHenry et al. 2000) suggest that a warm-start configuration is preferable to a cold start, and, thus, the former is used as a default. The warm start provides an estimate of the background concentrations of precursors and also of secondary pollutants. In the Sydney region remnant ozone on occasion is predicted to persist aloft, and the warm-start procedure provides a method to include this type of structure in the forecasts. No correction of the initial fields toward observations is performed at this time, because of the lack of sufficient data.

Output from the CTM is stored in machine-independent format and is postprocessed to provide images that are placed on a Web site (e.g., for daily updates of the Victorian forecasts see online at http://www.epa.vic.gov.au/Air/AAQFS). A daily verification cycle is also undertaken using the CTM output and real-time meteorological and air quality observations.

## 3. Performance

In this section we provide an initial assessment of AAQFS performance for the NWP and coupled NWP–EIM–CTM components. It is not yet possible to make an independent assessment of the EIM, although, for Victoria, the fleet-average motor vehicle emissions are in good agreement with observations (EPA Victoria 1999).

In considering performance criteria it must be recalled that key components of the system were untried (EIM, CTM) prior to the demonstration period or had not been extensively exercised for the conditions of most relevance to AAQFS. For example, although the NWP has been in operation since 1996, AAQFS represents a first application in forecasting worst-case mesoscale air pollution meteorological conditions. Similarly, use of AAQFS to generate urban- and regional-scale particle forecasts represents the first comprehensive attempt to undertake detailed inventory and transport modeling of this air pollutant group in Australia. Given this situation, all aspects of system performance (not just forecasting performance) have been examined. As a result, the demonstration period has been one during which the system has continued to evolve, because issues were identified and then addressed by the AAQFS team.

### *a. Meteorological performance*

The performance of the NWP has been assessed through comparison of observed and modeled wind, temperature, humidity, mixing height, and ventilation fields. Performance has been characterized through the use of statistical measures and also through a qualitative review of the ability of the NWP to reproduce key spatial features in the meteorological fields. For example, as discussed in Tory et al. (2004), the accurate prediction of air parcel trajectories during photochemical smog episodes in Melbourne requires that the NWP reproduce the characteristic spatial flow patterns associated with the Melbourne eddy, the Port Phillip bay breeze, and the Bass Strait sea breeze. Similar considerations are also evident for the forecasting of photochemical smog episodes in NSW (Hess et al. 2004).

Considering the use of statistical measures of NWP performance, we quantify the veracity of the near-surface wind forecasts using a single variable called the wind index. The wind index is essentially the vector root-mean-square (rms) error for the wind at 10-m height. It is calculated by taking the square root of the sum of the squares of the rms errors between the modeled values and the measured values from the aviation routine weather report (METAR)/surface synoptic observations (SYNOP) network of the wind components $u$ and $v$. The wind index is averaged over all stations in the domain and over 24 h. Similarly, the temperature index is a single variable that characterizes the performance of the near-surface temperature. It is calculated by taking the square root of the sum of the rms errors between the modeled values and the measured values from the METAR/SYNOP network for the screen temperature and screen dewpoint temperature. It also is averaged over the entire domain and over 24 h. The wind and temperature indices for the Victorian domain for the period from January to the middle of May 2001 are shown in Figs. 3a and 3b, respectively. Results are summarized in Table 1 for both the Victorian and NSW domains.

The results indicate that, in general, the LAPS model performs very well, and the performance is consistent over the whole period. The performance fluctuates because of the variation of the modeling difficulty with different weather systems and the variation of errors in the initial conditions. Larger excursions from the mean value in the temperature index are associated with the difficulty in forecasting rainfall and initializing the soil moisture. The trend in the indices is attributable to seasonal changes, with the weather being more variable during the summer.

Figure 3c shows the wind and the temperature indices for the upper air for Victoria (see Table 1 for NSW). In this case the indices represent the errors between the modeled values and the measured values along the three-dimensional flight path of commercial aircraft taking off from Melbourne Airport (AMDAR data). The wind index represents the vector wind rms error and the temperature index is the rms temperature error; there are no dewpoint temperature measurements available for the flights. The indices are averaged over all heights up to 5000 m and over 24 h (but the averages are weighted toward daylight hours because there are few flights overnight).

The results shown in Fig. 3c are similar to those in Figs. 3a and 3b, except that the upper-air wind errors are larger than those near the surface. This is expected because the wind speed increases with height. The upper-air temperature errors are smaller than those near the surface. There are two reasons for this. First, the upper-air temperature index does not contain the dewpoint temperature, which is more difficult to model than the dry-bulb temperature. Second, the upper air is thermally stably stratified to a greater extent than that near to the surface. There is a trend for decreasing rms errors with time, which we attribute to seasonal changes.

The ventilation is displayed in Fig. 3d. Ventilation is the product of the height of the planetary boundary layer and the average wind speed within the planetary boundary layer. This variable is an important predictor of air pollution potential. It quantifies the amount of mixing available to dilute pollutant concentrations. Smaller values of ventilation indicate higher pollution potential.

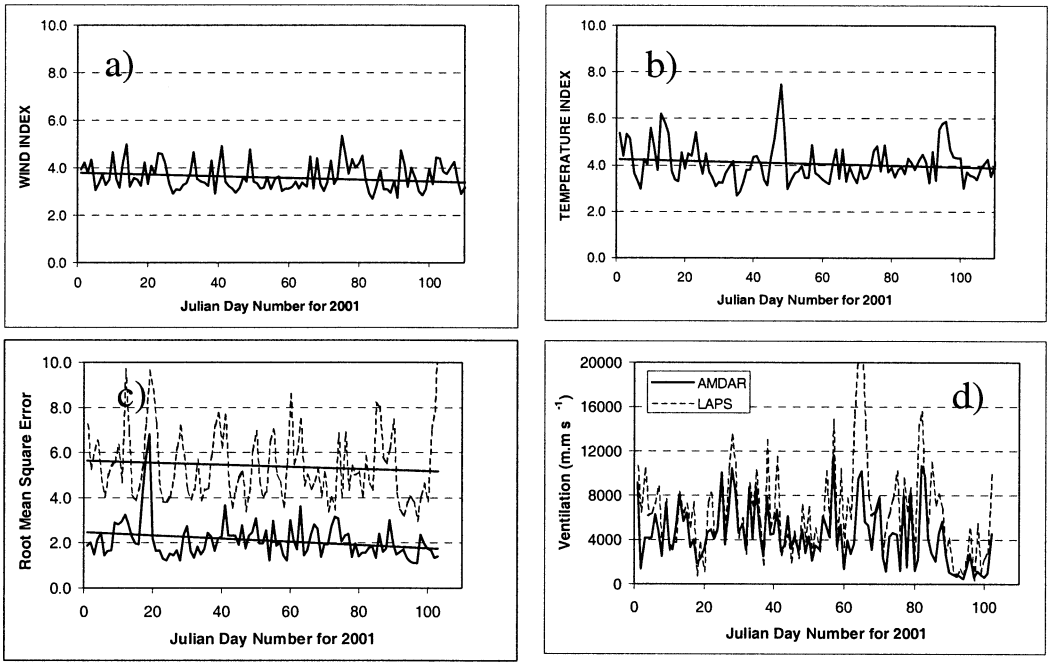


FIG. 3. NWP performance indices for Victoria, Jan–May 2001: (a) wind index, showing 10-m vector wind rms error; (b) temperature index, showing rms error for both screen temperature and screen dewpoint; (c) wind (dotted) and temperature (solid line) indices along the flight paths of commercial aircraft; and (d) comparison of modeled (LAPS) and measured (AMDAR) values of ventilation.

The comparison of the modeled and observed values shown in Fig. 3d shows that the ventilation trends are quite well captured by the model. There is a small bias for the model to overpredict the ventilation because of a slight bias toward dryness in the model. Further details on NWP performance are given in Manins (2001).

### *b. Air pollution performance*

Using air quality forecasting data generated during the demonstration period, we undertook a hierarchical review of system performance, commencing with a review of performance in reproducing key diurnal, monthly, and seasonal features (also see Manins 2001; Manins et al. 2002). This was evaluated through comparison of observed and modeled pollutant time series (using 1-h average data), through consideration of bias statistics, and through comparison of observed and modeled concentration frequency distributions. Examples in which frequency distributions are used to infer gross issues with model performance are given in the next section. Consideration is then extended to the system performance in forecasting peak daily concentration (using scatterplots, bias statistics, and contingency metrics). This approach is discussed in section 3b(2).

#### 1) FREQUENCY DISTRIBUTIONS

When long-term time series of pollutant concentrations are available, it has been recommended (Seigneur

TABLE 1. Statistical summary of NWP performance for the Victorian and NSW domains for the period from Jan 2001 to the first half of May 2001.

| | Mean bias | | Mean correlation | |
|---|---|---|---|---|
| Variable | Victoria | NSW | Victoria | NSW |
| $u$ component (m s$^{-1}$) at 10 m | −1.12 | −0.27 | 0.60 | 0.56 |
| $v$ component (m s$^{-1}$) at 10 m | 0.22 | 0.06 | 0.59 | 0.54 |
| Screen temperature (°C) | 1.11 | 1.31 | 0.87 | 0.89 |
| Screen dewpoint temperature (°C) | 0.24 | −0.11 | 0.66 | 0.77 |
| | Wind index (m s$^{-1}$) | | Temperature index (°C) | |
| Mean rms error (METAR/SYNOP comparison: near-surface data) | 3.57 | 3.37 | 4.04 | 3.96 |
| Mean rms error (AMDAR comparison: upper-air data) | 5.33 | 4.95 | 2.12 | 1.65 |

et al. 2000) that frequency distributions of observed and modeled concentration be compared to assess model performance in reproducing observed characteristics such as the mean, mode, and variational properties. Similarly, we have found that a comparison of the upper percentiles of observed and modeled concentration may be used to identify systematic errors or gross deficiencies in the forecast concentration fields.

Plots of observed and modeled concentration percentiles (50th, 90th, 95th, 99th, 99.9th, and 100th) for $O_3$, $NO_2$, $NO_y$ ($NO_y = NO_x +$ other nitrates; $NO_x = NO + NO_2$), $SO_2$, and PM10 are presented in Figs. 4a–4d for Port Phillip for March 2001 and June–July 2001, corresponding to the last month of the photochemical smog season, and 2 months of winter dispersion conditions. Plots for the Sydney basin are given in Manins (2001).

Considering $O_3$ and referring to Figs. 4a and 4b, it can be seen that the agreement between observed and forecast percentiles is excellent, particularly at the higher percentiles. The seasonal variation is also well reproduced, although this is a robust feature that is forced by the lower temperatures and radiation in the winter months. There is a trend to overpredict the observed ozone concentration at the lower percentiles during the summer period. The primary cause is a 5–10-ppb overprescription of the background $O_3$ concentration in unpolluted maritime flows (25 vs 15–20 ppb). The reason lies with the GRS mechanism—ozone destruction under conditions of low $NO_x$ and high water vapor concentration is not modeled by the mechanism.

Referring to Figs. 4c and 4d it can be seen that $NO_2$ is overpredicted at the higher percentiles (e.g., the normalized bias increases from 6% at the 50th percentile to 57% for the maximum concentration). This trend was also observed by Carruthers et al. (2000) when modeling the London, United Kingdom, urban plume using the Urban Advanced Dispersion Modeling System (ADMS-Urban) with GRS photochemistry (annual 1-h maxima were overpredicted by 400% on the average in that study). For the Australian modeling, the cause is a systematic overestimate of the initial reactivity of the urban air mass by the highly condensed GRS photochemical mechanism.

The observed–modeled percentile plot for $NO_y$ is shown in Figs. 4e and 4f. It can be seen that the system has generally been able to reproduce the observed distribution with only a small bias for all of the percentile levels. The system has successfully reproduced the interseasonal variation, with peak $NO_y$ concentrations increasing by more than a factor of 2 between summer and winter (an outcome that is inverted in comparison with ozone). This is due to the existence of lower ventilation rates in the Port Phillip airshed during winter. The mean normalized bias varies between 3% and 17%—a result that compares well to the work of Hurley (2000), who modeled Melbourne's air quality for a 1-month period (December 1998) using a prognostic meteorological air quality model that is driven by analyzed meteorological fields rather than forecast fields. He found a bias of the all-station mean observed and predicted 99.9th percentile of $-7.8\%$, and a bias for the maximum $NO_y$ concentration of only $-1\%$. A 1-yr simulation of air quality in London undertaken by Carruthers et al. (2000), using the ADMS urban model, also yielded similar results, with mean biases for the average 98th, 99th, and 100th percentile 1-h $NO_y$ concentrations lying within the range $+1\%$ to $-20\%$. Thus, AAQFS, when operating in forecast mode, performs similarly to models that have either been driven by 6-hourly meteorological analyses or by meteorological observations.

The $SO_2$ percentile plots for Alphington (Figs. 4g,h) are indicative of the generally low $SO_2$ concentrations that are present in urban Melbourne. On the other hand, the Paisley monitoring station, which is located within the vicinity ($\sim$1 km) of a large industrial complex, occasionally observed 1-h $SO_2$ peaks of greater than 50 ppb during the study period. It can be seen that AAQFS has had difficulties in matching the highest observed $SO_2$ concentrations. This is because the 1-km AAQFS urban grid cannot adequately resolve the point-source $SO_2$ plumes responsible for the observed peaks. This is likely to be an ongoing issue with the forecasting of peak $SO_2$ concentration in both Melbourne and Sydney. Given the low levels of sulfur present in Australian fuels, the forecasting issue is reduced to one of predicting near-source impacts downwind of industrial complexes. The use of alternative models and/or subgrid-scale modeling may be required for this situation.

Observed and predicted percentiles for the cumulative frequency distributions of 1-h PM10 are shown Figs. 4i and 4j, respectively, for summer and winter periods. In comparing the results, it should be recalled that major contributors in the warm, dry months are coarse fraction particle sources, such as bushfire smoke, windblown dust, sea salt aerosol, and secondary nitrate aerosol. During the cooler, wetter winter months these sources are substantially reduced and are replaced in dominance by wood smoke from domestic wood combustion for heating (EPA Victoria 1999). Emissions from the motor vehicle fleet contribute approximately equally to both seasons (although secondary particle production from gaseous pollutants will be higher in the summer).

From Fig. 4i it can be seen that there is a reasonable level of agreement between the system and observations during the summer month (March). Note that these results were achieved without the windblown dust and bushfire modules in operation. However, analysis of the timing of the observed peaks and ratio of PM2.5 to PM10 suggests that motor vehicles were the dominant source during this period.

During the winter period it can be seen (Fig. 4j) that observed concentrations of PM10 have been overpredicted for all levels at, and above, the 90th percentile. A sensitivity study demonstrated that the domestic wood combustion particle source was the likely candidate for

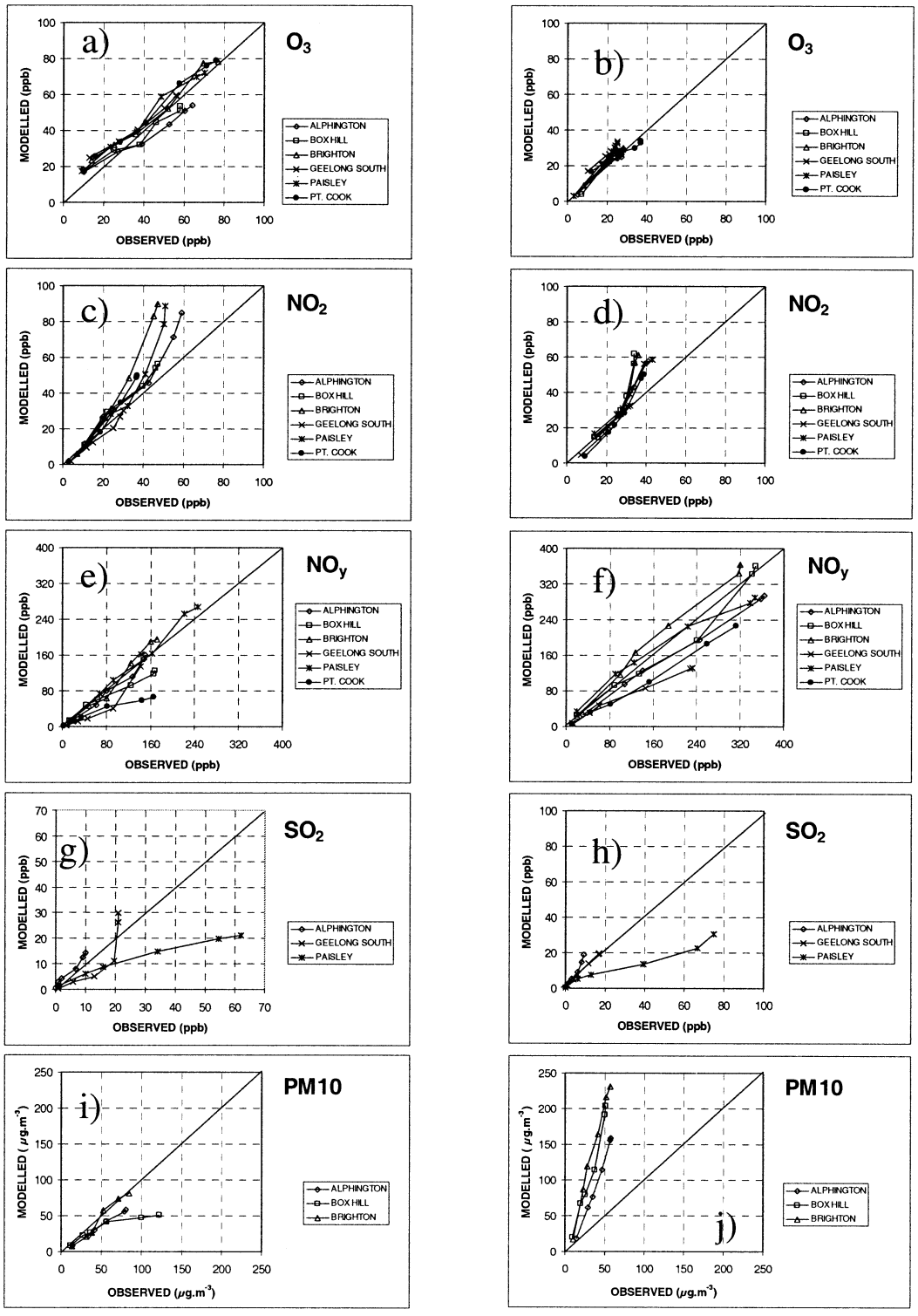


FIG. 4. Plots of observed and modeled 50th, 90th, 99th, 99.9th, and 100th percentile concentrations for Melbourne: (a) $O_3$ summer, (b) $O_3$ winter, (c) $NO_2$ summer, (d) $NO_2$ winter, (e) $NO_y$ summer, (f) $NO_y$ winter, (g) $SO_2$ summer, (h) $SO_2$ winter, (i) PM10 summer, and (j) PM10 winter.

the strong overprediction of PM10 during the winter months and the emission factors were identified as having the greatest level of uncertainty. A review of recently published emission factors (i.e., Fine et al. 2001) has resulted in the adoption of a revised set of factors that are one-half to one-third times those used in AAQFS during the demonstration period.

### 2) FORECASTS OF DAILY MAXIMUM CONCENTRATION

The evaluation presented in the previous section was undertaken in order to examine the ability of the system to reproduce the observed monthly cycles of concentration and to identify areas (such as the particle modeling) that needed further refinement. However, the principal aim of the system is to provide forecasts of daily peak concentrations. In both Sydney and Melbourne, the principal pollutant of concern is $O_3$, with exceedances of the 1-h national 100-ppb standard observed in both cities. We provide here a preliminary review of the system's ability to forecast peak daily concentrations of $O_3$.

Presented in Fig. 5 and Fig. 6 are performance plots for the observed and forecast peak daily 1-h concentrations of $O_3$. Mean bias statistics are presented in Table 2. Consideration is given to two levels of performance, *coupled in space*, where observed and forecast maxima are compared on a station-by-station basis, and *uncoupled*, where the forecast maxima for the grid is compared with the observed network maxima. We consider both coupled and uncoupled comparisons because we are interested in exploring the issues involved in generating both suburban-level and airshed-scale air quality forecasts.

Scatterplots of observed and forecast daily peak 1-h $O_3$ are shown in Figs. 5a and 5b for Port Phillip (coupled and uncoupled) and in Figs. 6a and 6b for the Sydney basin (note the different concentration scales). Plots of fractional bias versus forecast concentration are given in Figs. 5c and 5d and Figs. 6c and 6d. The use of fractional bias follows the recommendations of Seigneur et al. (2000):

$$B_f = \frac{2}{N}\sum_{i=1}^{N}\left(\frac{P_i - O_i}{P_i + O_i}\right), \quad (1)$$

where $N$ is the number of model ($P_i$) and observation ($O_i$) pairs. Note that $B_f$ varies symmetrically between $-2$ and 2. A factor-of-2 difference between observed and modeled corresponds to a fractional bias of $\pm 2/3$ (0.667). Seigneur et al. also recommend the use of fractional gross error and the coefficient of determination (the square of the correlation coefficient). We have reported each of these statistics in Table 2.

From the ozone scatterplot for Port Phillip (Fig. 5a), it can be seen that a majority of daily peak 1-h ozone concentrations lie close to the background of 20–25 ppb. Peaks of less than 20 ppb correspond to periods of prolonged titration and/or deposition and peaks of greater than 25 ppb correspond to varying degrees of photochemical production. From Table 2 it can be seen that 96%–98% of forecast daily peak 1-h ozone concentrations lie within a factor of 2 of the observed. Taking the line of best fit as a guide, it can be seen that the system overpredicts at the lowest concentrations (as was noted in the section on frequency distributions). The coefficient of determination is 0.65, which compares well to the values reported by Draxler (2000) (0.24–0.49) and McHenry et al. (2000) (0.42).

On a small number of days, daily peak ozone concentrations of up to 80 ppb were observed in the Port Phillip region. These are the cases of most interest from a forecasting perspective. The bias plots (Figs. 5c,d) indicate that these cases were predicted with good skill. However, the fractional bias increases at the lower end of the concentration range in response to a systematic overprediction of daily maxima for near-background concentrations. The mean bias fractional bias is 0.10 (Table 2), which corresponds to a mean relative bias of only 10%. Performance measures improve for the spatially uncoupled case (although differences in sample size must also be taken into consideration).

Scatter- and bias plots for the Sydney basin are shown in Figs. 6a–d. Note that, in addition to the periods of March, June, and July 2001, we have also included results for an ozone episode spanning 21–27 January 2001 (this episode is discussed in detail in Hess et al. 2004). From Fig. 6a it can be seen that ozone concentration peaks of up to 180 ppb were observed by the DEC network. Although the system performs very well, there is a tendency to underpredict the highest peaks at individual stations, as evidenced by the slope of the regression line and the fractional bias plot (Fig. 6c). There is also more scatter than for Port Phillip, as evidenced by the smaller coefficient of determination and the larger fraction gross error (although all of these differences are also influenced by sample size). The enhanced level of scatter primarily occurs because the highest observed ozone concentrations are generated within the sea breeze. Large ozone concentration gradients exist across the sea-breeze front (with the contaminated air mass contained within the maritime flow). For some conditions of worst-case photochemical smog in Sydney, the sea-breeze ingress into the Sydney basin may be slowed or blocked for a number of hours by a strengthening offshore synoptic flow (Hess et al. 2004). Under these conditions, it is very challenging to correctly predict the time and location of the sea-breeze front, thus leading to occasional large errors in the station-coupled performance statistics. Relaxation of the spatial coupling criteria leads to considerable improvement.

### 3) CONTINGENCY TABLES

A common approach for appraising forecasting performance is through the use of contingency tables,

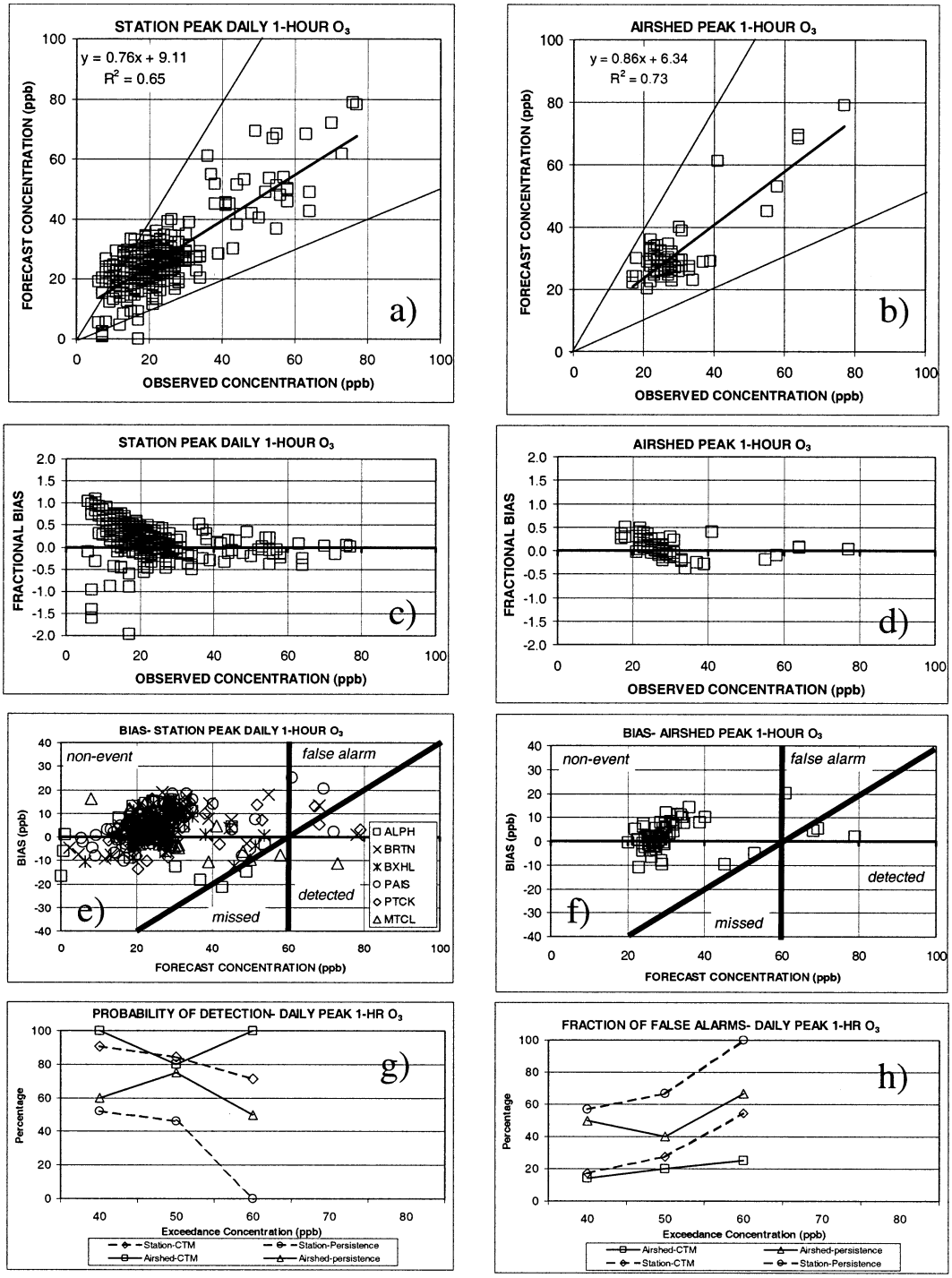


FIG. 5. Plot of performance statistics for Melbourne: (a), (b) space-paired and unpaired observed and forecast daily peak 1-h $O_3$ scatterplots; (c), (d) fractional bias vs observed daily peak; (e), (f) bias vs forecast daily peak; (g) probability of detection; (h) fraction of false alarms.

which tabulate the number of missed events, correct forecasts, and false alarms. Following the recommendation of De Leeuw (2000), we use two measures to quantify forecast performance. The probability of detection (SP) is given by the ratio of correct forecasts to the total number of observed exceedances. Similarly, the false-alarm rate (FR) is given by the ratio of non-observed forecast exceedances to the total number of forecast exceedances.

The relationship between bias and contingency is

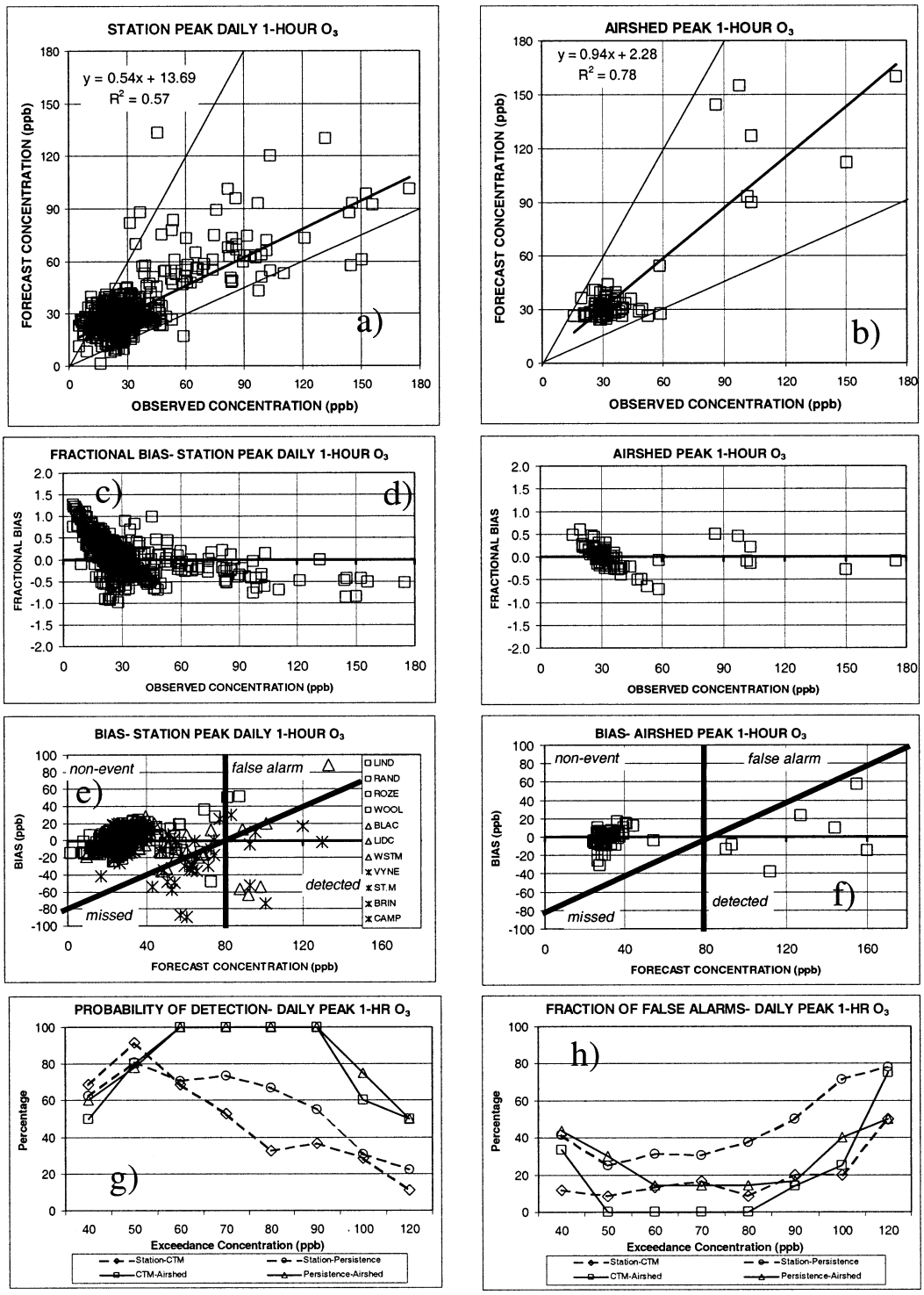


FIG. 6. Plot of performance statistics for Sydney: (a), (b) space-paired and unpaired observed and forecast daily peak 1-h $O_3$ scatterplots; (c), (d) fractional bias vs observed daily peak; (e), (f) bias vs forecast daily peak; (g) probability of detection; (h) fraction of false alarms. Note that data from monitoring stations in (e) are grouped according to distance inland from the coast.

TABLE 2. System forecasting performance for daily maximum 1-h ozone: Port Phillip and Sydney basin.

| | Coupled in space | | | | Uncoupled | | | |
|---|---|---|---|---|---|---|---|---|
| | Factor of 2 | Fractional bias | Gross error | Coef of determination | Factor of 2 | Fractional bias | Gross error | Coef of determination |
| Domain | | | | | | | | |
| Port Phillip | 0.96 | 0.10 | 0.26 | 0.65 | 0.98 | 0.07 | 0.16 | 0.73 |
| Sydney basin | 0.92 | 0.02 | 0.25 | 0.57 | 0.97 | −0.03 | 0.19 | 0.69 |

shown graphically in Figs. 5e and 5f (Port Phillip) for an exceedance concentration of 60 ppb, and in Figs. 6e and 6f (Sydney basin) for an exceedance concentration of 80 ppb. We have plotted daily station $O_3$ bias and airshed $O_3$ bias as a function of forecast daily peak 1-h $O_3$. These plots illustrate the impact of system bias on contingency table outcomes, and, for coupled-in-space results (Figs. 5e and 6e), highlight any systematic bias that may exist between locality and contingency performance. For example, the majority of the missed cases for the coupled Port Phillip daily peaks occur at the inland stations of Mount Cottrell and Alphington (see Fig. 1). Similarly, missed cases for the Sydney basin are also associated with inland sites, which may indicate a systematic flaw in the treatment of transport or chemical transformation away from coastal regions.

These results are further generalized in Figs. 5g, 5h, 6g, and 6h where we have plotted SP and FR as a function of $O_3$ exceedance concentration. Multiple exceedance levels have been used in order to provide insight into system performance as the peak concentrations become progressively more extreme. In assessing these results, some guidance as to the skill levels of contemporary forecasting systems is also available from De Leeuw (2000) (discussed below). De Leeuw also recommends that forecast performance be compared with that of a simple persistence model (i.e., the forecast pollutant concentration for day "$i$" is equal to the observed pollutant concentration on day "$i - 1$").

From a consideration of the spatially coupled results shown in Fig. 6g for the Sydney basin, it can be seen that the system and persistence have comparable detection rates at thresholds of 60 and 100 ppb. On the other hand, AAQFS has a reduced probability at the other threshold levels. For both approaches, the detection rates drop from 75% at a 60-ppb threshold to 10%–20% at a threshold of 100 ppb. In the case of the false-alarm rate, it can be seen that AAQFS performs substantially better than persistence, maintaining a station-level false-alarm rate of $<20\%$ for exceedence thresholds in the range of 40–100 ppb. False-alarm rates for the persistence model are typically double those of AAQFS. Both AAQFS and the persistence model perform better when spatial coupling is relaxed, with both approaches able to maintain a detection probability of 100% for exceedence thresholds in the range of 60–90 ppb. False-alarm rates for AAQFS are again lower for concentrations in the range of 40–100 ppb.

Note that the strong performance of the persistence model in this analysis for Sydney is, to some degree, dictated by the occurrence of a contiguous 7-day ozone episode during the study period. By definition, persistence will perform well under these conditions. AAQFS performed less well for the coupled-in-space detection probabilities because, as discussed previously, some of the most extreme ozone event days were characterized by a challenging balance between the offshore synoptic flow and the onshore sea breeze [see Hess et al. (2004) for discussion of these factors in a case study].

Bias and contingency plots for daily peak 1-h ozone forecasts in Port Phillip are presented in Figs. 5g and 5h. Again, results are shown for both station-level daily peaks and for airshed maxima. Although the system is yet to be tested for a full range of conditions, it can nevertheless be seen that both the probability of detection and the rate of false alarms for AAQFS are comparable or considerably better than that which can be achieved through persistence.

These initial results from the Port Phillip and Sydney basin ozone forecasts compare very favorably to other forecast systems. For example, DeLeeuw (2000) compared the results of three statistical models for a Dutch ozone forecasting system. When forecasting the exceedances of 60 ppb, three alternative models recorded detection probabilities in the range of 30%–70% and probabilities of false alarm in the range of 14%–63%. At a 60-ppb exceedance threshold, AAQFS achieved a detection probability of 70% for local-level forecasts and 100% for the forecast of airshed maxima in Port Phillip. In the Sydney basin, the detection probabilities were also 70% and 100%, respectively. The false-alarm rates are 50% and 30% for Port Phillip and 45% and 25% for Sydney. The most important cause for the systematic error of the forecasts in both Melbourne and Sydney is the difficulty in predicting the meteorological conditions accurately (Hess et al. 2004; Tory et al. 2004). Errors in the emissions inventory are thought to be less important; however, some uncertainty remains in the specification of biogenic emissions. The simple, compressed chemistry mechanism used in the forecasts can underestimate peak ozone values on occasion (Tonnesen and Jeffries 1994).

These results also compare well to those reported by Cardelino et al. (2001) for a study in which four numerical methods and a 10-person team were used to forecast 8-h ozone peaks for the Atlanta, Georgia, region

for the 1999 ozone season. Two regression models, persistence and an NAQFS, made up the numerical forecasting methods. Forecasts from the models were then provided to the forecasting team and combined with experience and intuition, and a ''team forecast'' was generated. The models achieved detection probabilities in the range of 75%–85%, and false-alarm rates in the range of 16%–28%. A statistical regression model provided the most skillful forecast, the persistence model had the lowest probability of detection, and the NAQFS had the highest number of false alarms. The team performance was comparable to the best model. The NAQFS was considered to have the greatest potential for improvement, having the highest systematic error component (as compared with a nonsystematic or random error).

## 4. Discussion and conclusions

Although the performance dataset is currently small, it can nevertheless be seen that AAQFS shows good promise for the forecasting of ozone. With the exception of the space-coupled performance for Sydney basin, results are superior to persistence. With respect to primary gaseous pollutants, typical noise levels for the prediction of daily peaks are about a factor of 2 (Manins 2001). The particle modeling is at a preliminary stage, with work still under way on the configuration and refinement of the source emission modeling. However, forecasts for motor-vehicle-dominated scenarios are promising.

An additional, less-quantifiable feature of AAQFS (and of an NAQFS, in general) is the insight that the system can provide into the dynamics of pollutant buildup and transport. For example, AAQFS predicts the transport of significant concentrations of photochemical smog well beyond existing monitoring networks in Melbourne and Sydney. The system has highlighted the importance of the Sydney southerly buster (cold front) as a mechanism for the transport of the Sydney urban photochemical smog plume to the central coast and the city of Newcastle, 100 km to the north (confirmed by observations in the Newcastle region). The system has been able to model a significant smoke impact in Melbourne from a bushfire on King Island located more than 200 km to the south (Lee et al. 2002). Last, the system has provided an important, ongoing feedback mechanism into the veracity of the meteorological and emissions modeling, both being systems that have important uses outside of the air quality forecasting field.

The results of the photochemical smog modeling have been achieved using a highly simplified photochemical mechanism (GRS), which provides a trade-off between computational speed and chemical detail/robustness. Operation of AAQFS with GRS has enabled the use of large and high-resolution (1 km over the urban areas) forecasting domains, thus providing the joint potential to provide suburban-, urban-, and regional-scale forecasts within the existing operational computational and time constraints of the operational weather forecasting system. We are currently in the process of evaluating the operation of AAQFS using the CB-IV mechanism. Initially CB-IV will be used to investigate ozone episodes in a nonforecast mode. However, subject to the availability of computational resources, it is anticipated that the CB-IV mechanism will eventually be used extensively in an operational forecasting mode. The forecasting of secondary aerosols, including the organic component, is a goal for the future, and this will require a sophisticated chemical mechanism (Griffin et al. 2002).

Further improvement to primary pollutant forecasts will be sought through improved representations of the urban boundary layer. A windblown dust emission module has been incorporated into AAQFS and is undergoing testing against historical case studies with good promise. This module will shortly be incorporated into the daily forecasts. With respect to the wildfire algorithm, the goal is to use AAQFS to forecast the impact of fires that have been burning prior to and possibly during the forecasting period. The challenge now is to automate the process for generating bushfire characteristics data. For example, in early January 2002 Sydney experienced large-scale bushfires, leading to significant particle loading within the Sydney basin. Photochemical smog concentrations were also elevated, with the 1-h time series often displaying noncharacteristic temporal profiles. This suggests that $NO_x$ and VOC emissions from the bushfires may have contributed to photochemical smog production.

An important ongoing task will be to try to establish the limits of predictability of AAQFS. For example, it has been noted that the accurate forecasting of spatial locality for photochemical peaks is challenging in Sydney. A similar situation has been identified from historical case-study modeling in Port Phillip. Ensemble modeling provides one option for determining the sensitivity of plume location to initial conditions. We also need to look further at the relationship between spatial coupling and forecast accuracy. For example, we need to establish whether, in the event that coupled forecasts are considered too inaccurate, a semicoupled forecast (i.e., forecasting for subregions) will provide a result that has both acceptable accuracy and acceptable spatial discrimination.

*Acknowledgments.* The Australian Air Quality Forecasting System was funded in part by the Air Pollution in Major Cities Program (sponsored by Environment Australia through the Natural Heritage Trust).

REFERENCES

Adelman, Z. E., 1999: A reevaluation of the carbon bond-IV photochemical mechanism. M.S. thesis, Department of Environmental Sciences and Engineering, School of Public Health, University of North Carolina, 194 pp.

Azzi, M., G. J. Johnson, and M. E. Cope, 1992: An introduction to the Generic Reaction Set photochemical smog mechanism. *Proc.*

*11th Int. Clean Air Conf.*, Brisbane, QLD, Australia, Clean Air Society of Australia and New Zealand, 451–462.

Brandt, J., H. J. Christensen, L. M. Frohn, F. Palmgren, R. Berkowicz, and Z. Zlatev, 2001: Operational air pollution forecasts from European to local scale. *Atmos. Environ.*, **35,** S91–S98.

Cardelino, C., and Coauthors, 2001: Ozone predictions in Atlanta, Georgia: Analysis of the 1999 ozone season. *J. Air Waste Manage. Assoc.*, **51,** 1227–1236.

Carruthers, D. J., H. A. Edmunds, A. E. Lester, C. A. McHugh, and R. J. Singles, 2000: Use and validation of ADMS-urban in contrasting urban and industrial locations. *Int. J. Environ. Pollut.*, **14,** 364–374.

Cope, M. E., and D. Hess, 1998: The application of an integrated meteorological air quality modelling system to a photochemical smog event in Perth Australia. *Air Pollution Modeling and Its Application XII,* S.-E. Gryning and H. Chaumerliac, Eds., Plenum Press, 609–615.

De Leeuw, F., 2000: Criteria for evaluation of smog forecast systems. *Environ. Monit. Assess.*, **60,** 1–14.

Dewundege, P., 2001: A semi automated expert system for smog forecasting over Melbourne airshed. *Clean Air,* **35,** 35–40.

Draxler, R. R., 2000: Meteorological factors of ozone predictability at Houston, Texas. *J. Air Waste Manage. Assoc.*, **50,** 259–271.

EPA Victoria, 1999: Air emissions inventory, Port Phillip region. EPA Victoria Publ. 632, 48 pp.

——, 2000: Melbourne mortality study. Effects of ambient air pollution on daily mortality in Melbourne 1991–1996. EPA Victoria Publ. 709, 118 pp.

Ferguson, S. A., D. V. Sandberg, and R. Ottmar, 1998: Wild-land biomass emissions affected by land-use changes. Preprints, *Second Symp. on Fire and Forest Meteorology,* Phoenix, AZ, Amer. Meteor. Soc., 71–74.

Fine, P. M., G. R. Cass, and B. R. T. Simoneit, 2001: Chemical characterization of fine particle emissions from fireplace combustion of woods grown in the northeastern United States. *Environ. Sci. Technol.*, **35,** 2665–2675.

Gery, M. W., G. Z. Whitten, J. P. Killus, and M. C. Dodge, 1989: A photochemical kinetics mechanism for urban and regional scale computer modeling. *J. Geophys. Res.*, **94,** 12 925–12 956.

Griffin, R. J., D. Dabdub, and J. H. Seinfeld, 2002: Secondary organic aerosol 1. Atmospheric chemical mechanism for production of molecular constituents. *J. Geophys. Res.*, **107,** 4332, doi: 10.1029/2001JD000541.

Harley, R. A., A. G. Russell, G. J. McRae, G. R. Cass, and J. H. Seinfeld, 1993: Photochemical modeling of the southern California air quality study. *Environ. Sci. Technol.*, **27,** 378–388.

Hess, G. D., M. E. Cope, S. Lee, P. C. Manins, G. A. Mills, K. Puri, and K. Tory, 2000: The Australian Air Quality Forecasting System. *AMOS Bull.*, **13,** 67–73.

——, K. J. Tory, M. E. Cope, S. Lee, K. Puri, P. C. Manins, and M. Young, 2004: The Australian Air Quality Forecasting System. Part II: Case study of a Sydney 7-day photochemical smog event. *J. Appl. Meteor.*, **43,** 663–679.

Hurley, P., 2000: The Air Pollution Model (TAPM): Summary of some recent verification work in Australia. *Proc. 15th Int. Clean Air and Environment Conf.,* Brighton Beach, NSW, Australia, Clean Air Society of Australia and New Zealand, 90–103.

Lee, S., M. Cope, K. Tory, D. Hess, and L. Ng, 2002: The Australian Air Quality Forecasting System: Modelling of a severe smoke event in Melbourne, Australia. *Air Pollution Modelling and Its Application XV*, C. Borrego and G. Schayes, Eds., Kluwer Academic/Plenum, 95–114.

Lu, H., and Y. Shao, 2001: Toward quantitative prediction of dust storms: An integrated wind erosion modelling system and its applications. *Environ. Modell. Software,* **16,** 233–249.

Manins, P. C., 2001: Air quality forecasting for Australia's major cities—Final report. Project Management Committee, CSIRO Atmospheric Research, 341 pp. [Available online at http://www.dar.csiro.au/information/aaqfs.html.]

——, M. E. Cope, G. D. Hess, P. F. Nelson, K. Puri, N. Wong, and M. Young, 2002: The Australian Air Quality Forecasting System: Prognostic air quality forecasting in Australia. *Clean Air,* **36,** 43–48.

McHenry, J. N., N. Seaman, C. Coats, D. Stauffer, A. Lario-Gibbs, J. Vukovich, E. Hayes, and N. Wheeler, 2000: The NCSC-PSU numerical air quality prediction project: Initial evaluation, status, and prospects. Preprints, *Symp. on Atmospheric Chemistry Issues in the 21st Century*, Long Beach, CA, Amer. Meteor. Soc., 95–102.

Monahan, E. C., E. Spiel, and K. L. Davidson, 1986: A model of marine aerosol generation via whitecaps and wave disruption. *Ocean Whitecaps and Their Role in Air–Sea Exchange Processes*, E. C. Monahan and G. Mac Niocaill, Eds., Reidel, 167–174.

Morgan, P., 1986: Forecasting air pollution episodes in Melbourne. *Proc. Seventh World Clean Air Congress*, Vol. 2, Sydney, NSW, Australia, World Clean Air Congress, 315–322.

Nelson, P. F., P. C. Nancarrow, B. Halliburton, A. R. Tibbett, D. Chase, and T. Trieu, 2001: Biogenic emissions from trees and grasses. CSIRO Energy Technology Investigation Rep. ET/297, 63 pp.

Ng, Y. L., and M. Minchin, 2000: Spatial and temporal allocation of emissions from wood combustion. *Proc. 15th Int. Clean Air Environment Conf.,* Brighton Beach, NSW, Australia, Clean Air Society of Australia and New Zealand, 288–291.

——, S. Walsh, and N. Wong, 2000: Emissions model for the Australian Air Quality Forecasting System. *Proc. 15th Int. Clean Air Environment Conf.,* Brighton Beach, NSW, Australia, Clean Air Society of Australia and New Zealand, 275–280.

Ohara, T., A. Fujita, T. Kizu, and S. Okamoto, 1998: Advanced air quality forecasting system for Chiba Prefecture. *Air Pollution Modeling and Its Application XII*, S.-E. Gryning and H. Chaumerliac, Eds., Plenum Press, 625–633.

Puri, K., G. Dietachmayer, G. A. Mills, N. E. Davidson, R. A. Bowen, and L. W. Logan, 1998: The new BMRC Limited Area Prediction System, LAPS. *Aust. Meteor. Mag.*, **47,** 203–233.

Rufeger, W., P. Mieth, and T. Lux, 1997: Applying the DYMOS system in conurbations. *Proc. Modsim 97*, Vol. 4, Hobart, TAS, Australia, International Congress on Modelling and Simulation, 1797–1801.

Seigneur, C., and Coauthors, 2000: Guidance for the performance evaluation of three-dimensional air quality modeling systems for particulate matter and visibility. *J. Air Waste Manage. Assoc.*, **50,** 588–599.

Tonnesen, S., and H. E. Jeffries, 1994: Inhibition of odd oxygen production in the carbon bond four and generic reaction set mechanisms. *Atmos. Environ.*, **28,** 1339–1349.

Toon, O. B., R. P. Turco, D. Westphal, R. Malone, and M. S. Liu, 1988: A multidimensional model for aerosols: Description of computational analogs. *J. Atmos. Sci.*, **45,** 2123–2143.

Tory, K. J., M. E. Cope, G. D. Hess, S. Lee, K. Puri, P. C. Manins, and N. Wong, 2004: The Australian Air Quality Forecasting System. Part III: Case study of a Melbourne 4-day photochemical smog event. *J. Appl. Meteor.*, **43,** 680–695.

Venkatram, A., P. Karamchandani, P. Pai, and R. Goldstein, 1994: The development and application of a simplified ozone modeling system (SOMS). *Atmos. Environ.*, **28,** 3665–3678.

Walter, B., 1997: Combining ozone visualization with atmospheric light scattering. *Proc. Modsim 97,* Vol. 4, Hobart, TAS, Australia, International Congress on Modelling and Simulation, 1820–1826.